The Aerodynamics of a Cornering Inverted Wing in Ground Effect

James Keogh[1], Graham Doig[1], Tracie J. Barber[1], Sammy Diasinos[2]

[1]School of Mechanical and Manufacturing Engineering, University of New South Wales,

Sydney NSW 2052, Australia

[2]Science Faculty, Department of Engineering, Macquarie University

North Ryde NSW 2109, Australia

j.keogh@student.unsw.edu.au

Keywords: ground effect, cornering condition, inverted wing, aerodynamics, automotive aerodynamics, CFD

Abstract. For racing car configurations an inverted wing produces negative lift that allows increased levels of acceleration to be maintained through corners. Routine aerodynamic analysis, however, will typically be in the straight-line condition. A numerical analysis of the inverted T026 wing geometry through the curved path of a constant radius corner was conducted. The asymmetrical properties of the oncoming flow resulted in the introduction of a rolling and yawing moment along the span, as well as side-force. Yaw angle, flow curvature and a velocity gradient resulted in changes to the pressure distribution over the wing surface. Primary vortex behaviour was observed to differ significantly in both direction and structure.

Introduction

A front wing on a racing-car is operating in close proximity to the ground and will be subject to tight cornering manoeuvres. This negative-lift is most important when the car is accelerating. For most racing-cars this means that the predominant benefits are realised through the corners [1-4]. The downforce generated by the wing increases the available grip of the tyres and enables increased levels of acceleration to be sustained while the car remains on the track [2].

Although aerodynamic performance is most important in corners, designs will typically be evaluated through straight-line testing. This is due to wind tunnel testing being the primary design tool – and the inability it has to produce the curved flow of a corner. There is awareness within industry of the difference in the conditions experienced through a corner [3], however, the additional computational expense and inability to test experimentally results in this type of evaluation not being routine. The present work aims to identify the differences in aerodynamic performance and wake effects of an isolated inverted wing as it passes through a constant radius corner.
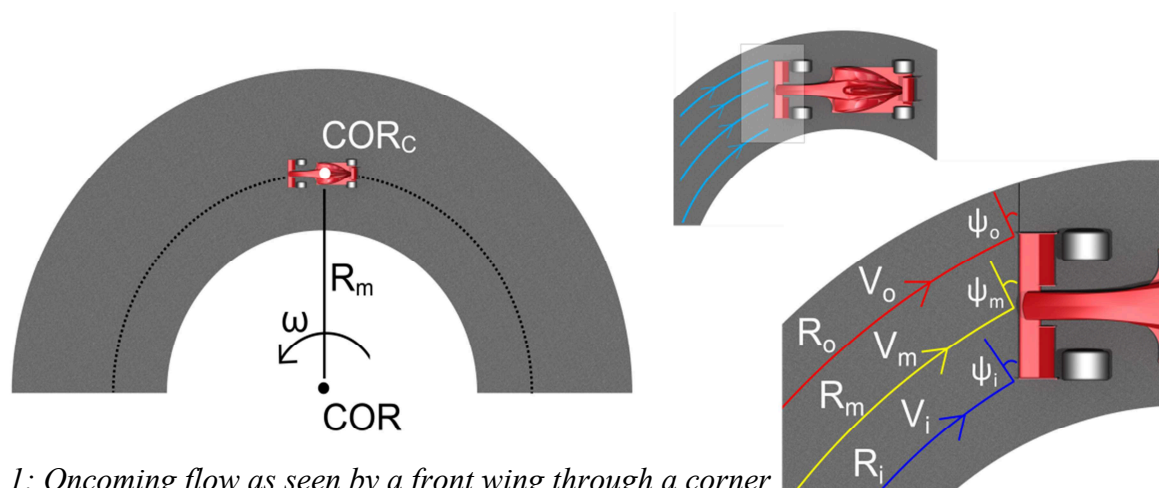

Fig. 1: Oncoming flow as seen by a front wing through a corner

In the field of ground effect aerodynamics an isolated inverted wing is one of the most commonly studied aerodynamic devices [5-9]. The present work utilises the T026 single element wing geometry experimentally investigated by Zerihan [7]. For an open-wheel type race-car the front wing is particularly important as it heavily influences all other components, and will be designed for downstream benefits.

Motion around a constant radius corner at a constant tangential velocity – therefore constant angular velocity – is being considered. This can be simplified as the body's centre of rotation (COR_c), rotating at a constant angular velocity (ω) about the centre of rotation (COR) of the corner – as is shown in Figure 1.

Considering the oncoming flow as seen by the front wing – the yaw angle and the flow curvature, along with velocity will vary along the length of the span. The outboard tip of the wing is in the highest velocity region (V_o) with the lowest yaw angle (ψ_o) and largest radius (R_o) of flow curvature. The adverse is true for the inboard tip.

From this it can be seen that:

$$R_o > R_m > R_i \; , \;\; V_o > V_m > V_i \;\; and \;\; \psi_o < \psi_m < \psi_i \tag{1}$$

Both velocity V and radius of curvature R will have a linear gradient along the length of the span. The variance between the values at the inboard tip to mid-span and mid-span to outboard tip will be equal. Curvature (κ) is defined as the inverse of R and varies according to this relationship – with the greatest curvature at the inboard tip and least at the outboard.

The effective yaw angle (ψ) of the flow, however, will vary proportional to the inverse tangent of the ratio between the wing distance forward of the car's centre of rotation (COR) and the curvature radius (R). This results in a greater variance in yaw angle occurring from the inboard tip to mid-span, than from mid-span to outboard.

Numerical Method

Fluent, a commercial finite-volume RANS solver, is commonly used within industry and was employed to generate all results presented. Steady-state solutions were obtained using the implicit, pressure- based coupled solver. All simulations were run in 64 bit double precision using a second-order upwinding discretization scheme for all equations. Simulations were run across 64 processes on the UNSW Trentino cluster. Convergence of solutions was monitored through both scaled-residuals errors and aerodynamic forces. Convergence was deemed to be met when aerodynamic forces ceased to vary by more than 0.01% for 1000 continued iterations and momentum scaled-residual errors ceased to change by 1% within the same period.

Recent work by Doig et. al [8] and Keogh et. al [10] demonstrate the appropriateness of the assumption of incompressibility at the velocities being considered in the present work. The x-velocity of the fluid relative to the wing geometry was set at a constant 30m/s, corresponding to a Reynolds number of 4.6×10^5. For validation cases a velocity inlet was set at a constant 30 m/s with a turbulence intensity of 0.2%. A pressure outlet with a zero static pressure was used as the outlet conditions. The walls for all simulations were modelled as slip, zero-shear walls. As the experiments were conducted with a moving ground, the ground was able to be modelled as stationary relative to the freestream fluid.

The four analysis cases used reference-frame motion to create the correct flow field. The velocity inlet was set at zero relative to the absolute reference frame,
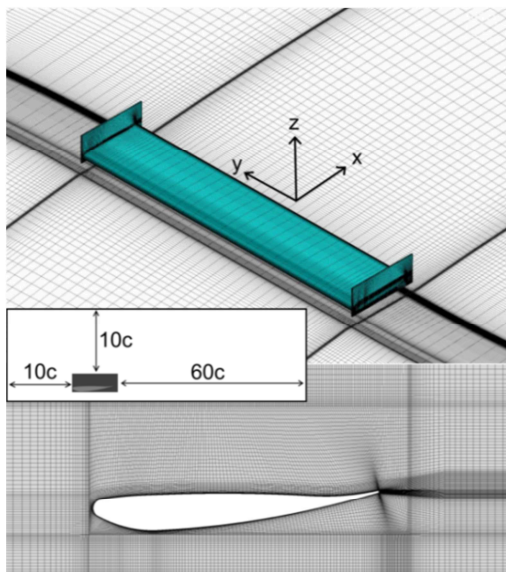

Fig. 2: Mesh construction and domain

along with the ground plane. Cornering cases used a constant angular velocity of 2.182 rad/s about a fixed point 61.55c from the centre of rotation in the *y*-direction. Straight-line and yaw cases utilised a translational velocity to create a relative freestream velocity of 30 m/s in the *x*-direction. Frame motion was compared to an inlet velocity in the stationary reference frame (for the straight-line condition) and was found to alter lift and drag values by approximately 0.01%.

For validation cases a domain of rectangular cross section (2.1x1.7m) was used – matching the dimensions of the Southampton Wind Tunnel used in the experiments of Zerihan [7]. The rectangular cross-section was used rather than octagonal due to the omission of a complete description – this may have affected results to a small degree. For validation the domain was extended 7c upstream and 15c downstream. A boundary sensitivity study subsequently determined that extending the domain downstream 60c and all other boundaries to a distance of 10c the flow was being sufficiently resolved and all aerodynamic forces ceased to be influenced. The larger domain extents were used for further analysis.
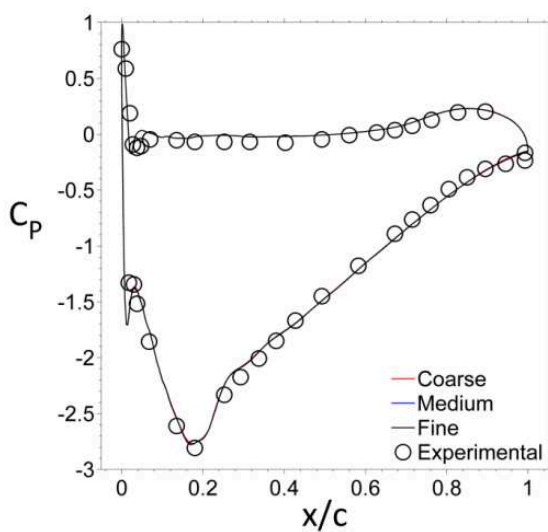

Fig. 3: Wing surface pressure distributions for coarse, medium and fine meshes

Table 1: Validation against experimental lift and drag values

	C_L	C_D
Experimental	*1.28*	*0.055*
Coarse	1.235	0.0568
Medium	1.236	0.0567
Fine	1.237	0.0567

Experimental results used a grit strip to fix transition at 0.1c from the leading edge. This was matched for validation cases with the use of a laminar zone at the leading edge. Subsequent cases for analysis assume a fully turbulent boundary layer. For the present study the ground clearance was fixed at h/c=0.179.

Validation and straight-line cases were run as semi-span models with a symmetry plane placed down the middle of the wing span. Yaw and cornering cases required the full wing geometry due to the asymmetry of the flow.

A structured mesh was generated using ANSYS ICEM 14.5. The domain consisted of hexahedral cells as shown in Figure 2. The wall y^+ value remained below 1 over the wing, endplate and ground. For cornering cases the domain was curved to match the flow curvature, additional care ensured the mesh aligned well with the direction of the flow for all cases.

A mesh convergence study determined the cell density required to accurately capture flow features. Validation was conducted against the lift and drag values obtained experimentally and surface pressure distributions taken at the centre of the wing span. The Realizable k-ε turbulence model with enhanced wall function was used for the mesh convergence study. The coarse, medium and fine meshes consisted of $1.9x10^6$, $3.5x10^6$ and $7.1x10^6$ cells respectively. Cells were primarily concentrated at the boundary, in the near wake and endplate intersection regions.
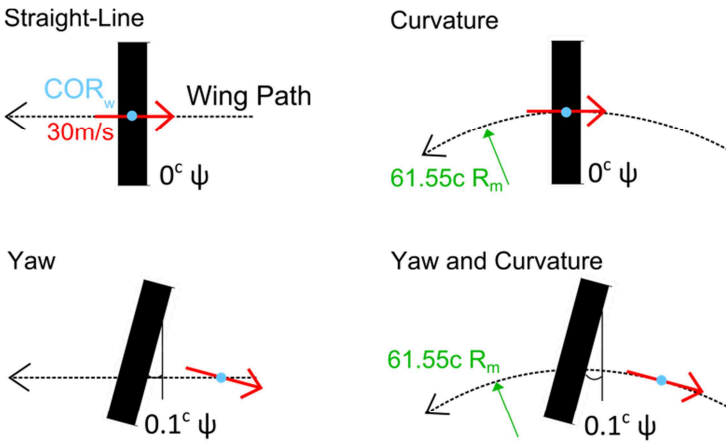
As can be seen in Table 1 all meshes under-predicted lift and over-predicted drag in comparison to the experimental results, with minor differences between. Figure 3 shows no real distinction in terms of the pressure distribution prediction at the mid-span location. All can be seen to match experimental results accurately.

Additional turbulence models were also assessed, but in agreement with previous studies [8,9] the Realizable k-ε model with enhanced wall function was found to be most suitable.

Fig. 4: Summary of four conditions analysed

Results

To better understand the complex flow seen by an inverted wing through a constant radius corner, four different conditions were assessed – shown in Figure 4. For all cases the velocity at the wing's centre of rotation and parallel to the direction of the wing's chord was 30m/s. All non-dimensionalisation was in reference to this value as a means of maintaining a reference point for evaluation. The straight-line condition was used as a baseline reference case. The second case considered a 61.55c (equivalent to 12.5 spans) radius turn. The third case considered a constant yaw angle of 0.1 radians. Finally, and most closely representative to true cornering, the wing maintained a position 6.175c forward of the centre of rotation, giving a yaw angle of 0.1 radians at the wing centre and a 61.55c radius of curvature at the centre of rotation.

A summary of force and moment coefficients for all cases is shown in Figure 5. Lift and drag varied by less than 0.2% across all cases. The yaw case demonstrates that the effects of the additional velocity component in the y-direction has little effect towards the net production of negative lift and drag for this particular geometry.
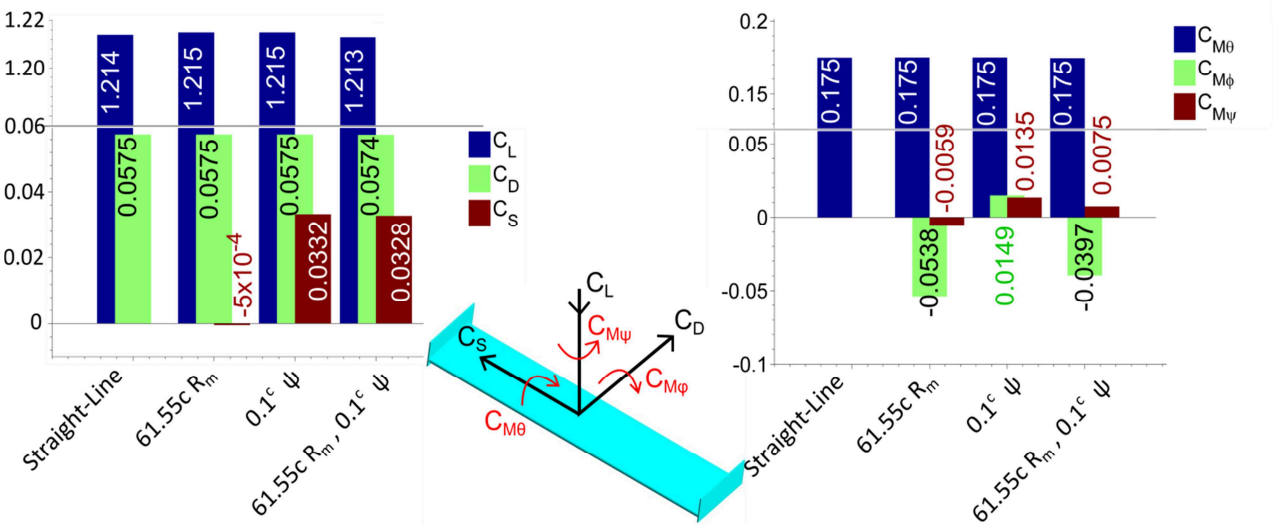

Fig. 5: Summary of aerodynamics forces experienced by inverted wing

For both cornering cases, a tangential velocity variance of 8% existed from the inboard tip to the outboard tip. A numerical study by Doig et. al [8] considered increased freestream velocities and found that this wing geometry maintained a slightly increasing lift coefficient value and slightly decreasing drag coefficient value – although both were very minor – for the ground clearance used in the present study. This demonstrates that the lift and drag values can be regarded as closely proportional to V^2. With a linear variance along the span – this would be expected to result in a small gain of 0.06% in the net production of both negative lift and drag (if the pressure distribution were to remain exactly proportional to velocity). This largely explains why, despite experiencing a spanwise velocity gradient, the overall lift and drag figures remained similar to those in the straight-line condition.

The addition of the flow component in the *y*-direction was found to result in a side-force for both cases experiencing a yaw angle. The *y*-component resulted in a high pressure region on the outside of the inboard endplate and pressure reduction on the inside. In both cases separation was observed at the leading edge of the outboard endplate due to the more substantial pressure gradient. For the yaw case, the side force contribution of the outboard endplate was 2.9 times than of the inboard. For the yaw and curvature case the outboard endplate had a 1.2% greater side force and 2.5% increased overall contribution to the side force coefficient. The seen flow at the outboard endplate was at a yaw angle 0.008^c (~0.46°) less than the inboard endplate, however the 8% higher velocity region resulted in a greater side force.

Figure 6 shows the difference in pressure distribution between the locations y/c=2.014 and y/c=-2.014 (the outboard distribution subtracted from the inboard). For the straight-line case the pressure distributions have zero difference due to symmetry properties. For the other three cases the asymmetry of the flow results in clear differences. For the curvature condition the outboard pressure distribution demonstrates an increase in magnitude due to a higher velocity in the oncoming flow (6.55% variance from y/c=2.014 to -2.014). This results in a difference profile that is visually very similar in shape to the wing surface pressure distribution. The asymmetry in lift and drag resulted in both a negative rolling moment and a negative yawing moment, as shown in Figure 5.
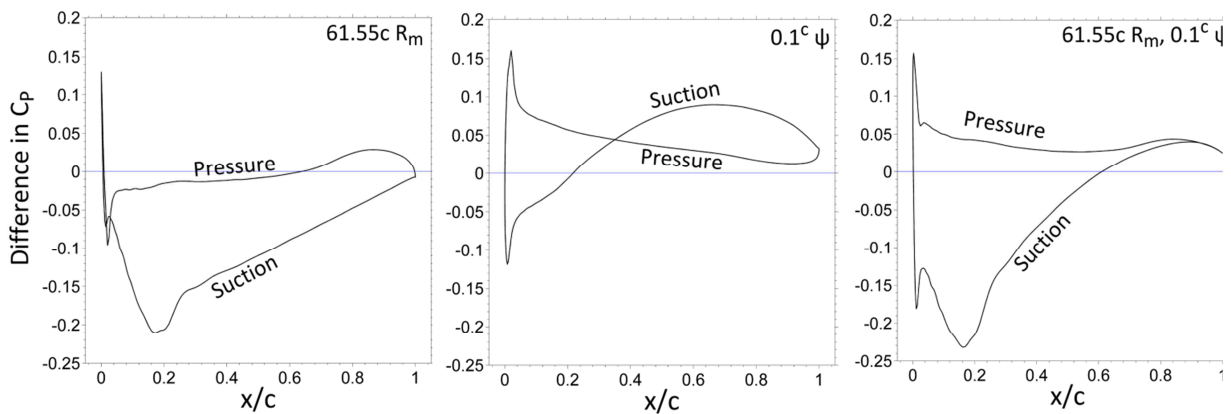

Fig. 6: Wing surface pressure distribution difference between y/c=2.014 and y/c= -2.014

For the yaw condition, the higher pressure inside the outboard endplate and lower pressure inside the inboard were seen to affect the pressure distribution at both y/c=2.014 and -2.014. Increased pressures in the pressure recovery region of the suction surface occured outboard – with the suction peak remaining unaffected. This produced a smaller positive rolling moment only 28% that of the curvature case. Increased outboard pressures resulted in a loss of strength of the lower vortex (refer to Figure 7) and increase in strength of the upper vortex. The opposite occured inboard, however the upper vortex changed to inside of the endplate due to the change in direction of the pressure gradient. The resultant drag imbalance along the span produced a larger positive yawing moment.

For the yaw and curvature condition the pressure recovery region of the suction surface closely resembled the sum of the curvature condition and yaw. A more significant outboard increase in the suction peak and increase in
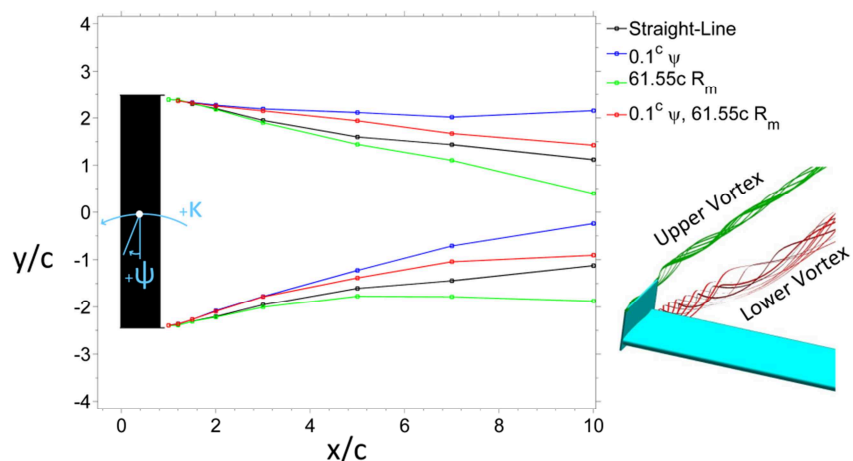

Fig. 7: Path of the lower vortices in the horizontal xy plane

the pressure spike at the stagnation point occured. Also a larger sustained pressure gradient difference from the leading edge occurred. Similar effects to the yaw case occurred in the near wake and resulted in rolling and yawing moments that closely reflected a summation of the curvature and yaw effects.

Accurate prediction of the vortical wake region is of high importance for downstream interactions. Figure 7 demonstrates the changes to the path of the lower vortices in the xy plane. The endplates acted as flow-straighteners in the near wake region causing the vortices to deviate from the direction of the freestream in the near wake region. Both yawed cases deviated more from the straight line condition in the near wake with the outboard vortex shifting by ~0.07c and inboard by ~0.13c at one chord-length downstream of the trailing edge. The curvature case remained initially less affected but displayed more significant changes further downstream. At 9c downstream (x/c=10) the outboard vortices were spread across a range of 1.8c in the *y*-direction and the inboard by 1.6c. As would be expected all vortices were affected by the different flow conditions to which they were exposed. Changes to the wake structure were also observed and continue to be of further invetigation.

Conclusion

An isolated inverted wing in ground effect has been investigated in four different flow conditions to identify the effects of cornering. For all conditions – other than the straight-line – a greater level of three-dimensionality was observed, both in forces acting on the wing itself and in the vortical wake created behind. These effects were the result of asymmetry in the oncoming flow seen by the wing. Effects of flow curvature, a velocity gradient and yaw were all observed to result in changes to the pressure distribution over the wing surface and the path of the prominent vortices generated at either end of the span. For a condition that is less severe than that of which modern race-cars are capable, results demonstrate significant changes to both the performance characteristics and wake.

References:

[1] Zhang X, Toet W and Zerihan J, 2006, "Ground effect aerodynamics of race cars," Applied Mechanics Review **59** pp. 33-49

[2] Katz J, 2006, "Aerodynamics of race cars," Annual Review of Fluid Mechanics **38**, pp. 27-63

[3] Toet W, 2013, "Aerodynamics and aerodynamic research in Formula 1," The Aeronautical Journal **117** pp. 1-26

[4] Dominy R G, 1992, "Aerodynamics of grand prix cars," Journal of Automobile Engineering **206** pp. 267-274

[5] Ranzenbach R and Barlow J, 1996, "Cambered aerofoil in ground effect – An experimental and computational study," SAE Paper No. 960909

[6] Katz J, "High-lift wing design for race-car applications," SAE Paper No. 951976

[7] Zerihan J, 2001, "An investigation into the aerodynamics of wings in ground effect," PhD thesis, University of Southampton

[8] Doig G, Barber T J and Neely A J, 2011, "The influence of compressibility on the aerodynamics of an inverted wing in ground effect", Journal of Fluids Engineering **133** (061102) pp. 1-12

[9] Diasinos S, Barber T J and Doig G, 2013, "Influence of wing span on the aerodynamics of wings in ground effect," Proceedings of the Institution of Mechanical Engineers, Part G: Journal of Aerospace Engineering **227** (3) pp. 569-573

[10] Keogh J, Doig G and Diasinos S, 2012, "The influence of compressibility effects in correlation issues for aerodynamic development of racing cars," 18th Australasian Fluid Mechanics Conference, Launceston, Australia, December